Phonon and crystal field excitations in geometrically frustrated rare earth titanates

T. T. A. Lummen,[1] I. P. Handayani,[1] M. C. Donker,[1] D. Fausti,[1] G. Dhalenne,[2] P. Berthet,[2]
A. Revcolevschi,[2] and P. H. M. van Loosdrecht[1,*]

[1]*Zernike Institute for Advanced Materials, University of Groningen, Nijenborgh 4, 9747 AG Groningen, The Netherlands*

[2]*Laboratoire de Physico-Chimie de l'Etat Solide, CNRS, UMR8182, Université Paris-Sud, Bâtiment 414, 91405 Orsay, France*

(Received 15 February 2008; revised manuscript received 17 April 2008; published 30 June 2008)

The phonon and crystal field excitations in several rare earth titanate pyrochlores are investigated. Magnetic measurements on single crystals of $Gd_2Ti_2O_7$, $Tb_2Ti_2O_7$, $Dy_2Ti_2O_7$, and $Ho_2Ti_2O_7$ are used for characterization, while Raman spectroscopy and terahertz time domain spectroscopy are employed to probe the excitations in the materials. The lattice excitations are found to be analogous across the compounds over the whole temperature range investigated (295–4 K). The resulting full phononic characterization of the $R_2Ti_2O_7$ pyrochlore structure is then used to identify crystal field excitations observed in the materials. Several crystal field excitations have been observed in $Tb_2Ti_2O_7$ in Raman spectroscopy, among which all of the previously reported excitations. The presence of additional crystal field excitations, however, suggests the presence of two inequivalent Tb^{3+} sites in the low-temperature structure. Furthermore, the crystal field level at approximately 13 cm^{-1} is found to be both Raman and dipole active, indicating broken inversion symmetry in the system and thus undermining its current symmetry interpretation. In addition, evidence is found for a significant crystal field–phonon coupling in $Tb_2Ti_2O_7$. The additional crystal field information on $Tb_2Ti_2O_7$ adds to the recent discussion on the low temperature symmetry of this system and may serve to improve its theoretical understanding.

DOI: 10.1103/PhysRevB.77.214310 PACS number(s): 75.50.Lk, 63.20.dd, 71.70.Ch, 75.30.Cr

I. INTRODUCTION

The term "geometrical frustration"[1–3] applies to a system when it is unable to simultaneously minimize all of its magnetic exchange interactions solely due to its geometry. Magnetically interacting spins residing on such lattices are unable to order into a unique magnetic ground state due to the competing magnetic interactions between different lattice sites. Instead of selecting a single, unique magnetic ground state at low temperatures, a pure magnetically frustrated system has a macroscopically degenerate ground state. In real systems, however, any secondary, smaller term (arising from single-ion or exchange anisotropy, further neighbor interactions, dipolar interactions, small lattice distortions, or a magnetic field, for example) in the system's Hamiltonian can favor certain magnetic ground states at very low temperatures, thereby (partially) lifting this peculiar degeneracy. In this fact lies the origin of the vast richness and diversity of the low-temperature magnetic behavior of different frustrated systems in nature.[1,4–7]

Geometries suitable for exhibiting frustration typically consist of infinite networks of triangles or tetrahedra, which share one or more lattice sites. One of the most common structures known that is able to induce magnetic frustration is that of the pyrochlores, $A_2B_2O_7$, where both the A^{3+} ions (rare earth element, coordinated to eight O atoms) and the B^{4+} ions (transition-metal element, coordinated to six O atoms) reside on a lattice of corner-sharing tetrahedra, known as the pyrochlore lattice. Thus, if either A^{3+} or B^{4+} is a magnetic species, frustration may occur due to competing interactions. A subclass of the pyrochlores is formed by the rare earth titanate family, $R_2Ti_2O_7$, where the R^{3+} ion is the only (para-)magnetic species, since Ti^{4+} is diamagnetic ($3d^0$). For the pyrochlore lattice, both theory[8–10] and Monte Carlo simulations[10,11] predict a "collective paramagnetic" ground state, or the lack of long-range magnetic ordering, for classical Heisenberg spins at finite temperature. The quantum Heisenberg spin ($S=1/2$) model for the pyrochlore lattice also predicts a quantum disordered system at finite temperatures, a state often referred to as a "spin liquid."[12] However, in reality the different perturbative terms in the corresponding Hamiltonian result in quite diverse low-temperature magnetic behaviors among the different rare earth titanates,[4] of which the Gd, Tb, Ho, and Dy variants are studied here.

The supposedly least complex case is that of gadolinium titanate, $Gd_2Ti_2O_7$. The Gd^{3+} ion has, in contrast to the Tb^{3+}, Ho^{3+}, and Dy^{3+} ions, a spin-only $^8S_{7/2}$ ($L=0$) ground state, rendering the influence of crystal field levels and possible induced Ising-type anisotropy insignificant in $Gd_2Ti_2O_7$. The experimentally determined Curie-Weiss temperature of $Gd_2Ti_2O_7$ is $\simeq -10$ K,[13–15] indicating antiferromagnetic nearest-neighbor interactions. Thus, $Gd_2Ti_2O_7$ could be considered as an ideal realization of the frustrated Heisenberg antiferromagnet with dipolar interactions. Experimentally, $Gd_2Ti_2O_7$ has been found to undergo a magnetic ordering transition at $\simeq 1$ K.[13] However, this transition corresponds to only partial ordering of the magnetic structure, as only three spins per tetrahedron order.[16] In this partially ordered state, the spins residing on the [111] planes of the crystal (which can be viewed as kagome planes) are ordered in a 120° configuration, parallel to the kagome plane, while the spins residing on the interstitial sites remain either statically or dynamically disordered.[17] Subsequent experimental investigations revealed a second ordering transition at $\simeq 0.7$ K, corresponding to the partial ordering of the interstitial disordered spins,[15,17] which, however, do remain (partially) dynamic down to 20 mK.[18,19] Despite that $Gd_2Ti_2O_7$ is supposedly well approximated by the Heisenberg antiferromag-

net with dipolar interactions, theoretical justification for this complex magnetic behavior remains difficult.[13,18,20]

In $Tb_2Ti_2O_7$, the dominant interactions are antiferromagnetic, as indicated by the experimentally determined Curie-Weiss temperature, $\theta_{CW} \simeq -19$ K.[21] A study of the diluted compound $(Tb_{0.02}Y_{0.98})_2Ti_2O_7$ revealed that the contribution to θ_{CW} due to exchange and dipolar interactions is $\simeq -13$ K, comparable to the θ_{CW} value found for $Gd_2Ti_2O_7$.[22] Despite the energy scale of these interactions, the Tb^{3+} moments do not show long-range magnetic order down to as low as 50 mK, making it the system closest to a real three-dimensional (3D) *spin liquid* to date.[21,23] However, crystal field (CF) calculations indicate a ground-state doublet and Ising-type easy axis anisotropy for the $(^7F_6)$ Tb^{3+} magnetic moments along their local ⟨111⟩ directions (the direction toward the center of the tetrahedron the particular atom is in), which would dramatically reduce the degree of frustration in the system.[22,24–27] Theoretical models taking this anisotropy into account predict magnetic ordering temperatures of about 1 K.[22,28] A subsequent theoretical work suggests that the magnetic moment anisotropy is more isotropic than Ising type, which could suppress magnetic ordering.[29] Recently, $Tb_2Ti_2O_7$ was argued to be in a quantum mechanically fluctuating "spin ice" state.[30,31] Virtual quantum-mechanical CF excitations (the first excited CF doublet is separated by only $\simeq 13$ cm^{-1} from the ground-state doublet[22,25,27]) are proposed to rescale the effective theoretical model from the unfrustrated Ising antiferromagnet to a frustrated *resonating spin ice* model. Nevertheless, the experimentally observed lack of magnetic ordering down to the millikelvin range and the true magnetic ground state in $Tb_2Ti_2O_7$ still remain enigmatic.[31–34]

Illustrating the diversity in magnetic behavior due to the subtle differences between the rare earth species of the titanates, the situation in both $Dy_2Ti_2O_7$ (Refs. 35–37) and $Ho_2Ti_2O_7$ (Refs. 38–41) is again different. The R^{3+} ions in these compounds have a $^6H_{15/2}$ (Dy^{3+}) and a $^5I_8$ (Ho^{3+}) ground state, respectively, with corresponding free ion magnetic moments $\mu = 10.65\mu_B$ (Dy^{3+}) and $\mu = 10.61\mu_B$ (Ho^{3+}). These systems were first thought to have weak ferromagnetic nearest-neighbor exchange interactions, as indicated by the small positive values of θ_{CW}, $\simeq 2$ and $\simeq 1$ K for $Dy_2Ti_2O_7$ and $Ho_2Ti_2O_7$, respectively.[42] More recently, however, the nearest-neighbor *exchange* interactions in $Dy_2Ti_2O_7$ and $Ho_2Ti_2O_7$ were argued to be *anti*ferromagnetic.[43] The effective ferromagnetic interaction between the spins in fact is shown to be due to the dominant ferromagnetic long-range magnetic dipole-dipole interactions.[28,44] The R^{3+} ions in both $Dy_2Ti_2O_7$ and $Ho_2Ti_2O_7$ are well described by a well separated Ising doublet (first excited states are at ~ 266 and ~ 165 cm^{-1}, respectively[24]) with a strong single-ion anisotropy along the local ⟨111⟩ directions. Unlike for antiferromagnetically interacting spins with local ⟨111⟩ Ising anisotropy, *ferro*magnetically interacting Ising spins on a pyrochlore lattice should be highly frustrated.[38,45] As Anderson[46] already pointed out half a century ago, the resulting model is analogous to the ice model of Pauling,[47] which earned both $Dy_2Ti_2O_7$ and $Ho_2Ti_2O_7$ the title "spin ice compound."[38,44,45,48] Although numerical simulations predict long-range order at low temperatures for this model,[43] experimental studies report no transition to a long-range ordered state for either $Dy_2Ti_2O_7$ (Refs. 28, 35, 49, and 50) or $Ho_2Ti_2O_7$ (Refs. 38, 51, and 52) down to as low as 50 mK.

As apparent from above considerations, the low-temperature magnetic behavior of the rare earth titanates is dictated by the smallest of details in the structure of and interactions in the material. Therefore, a comprehensive experimental study of the structural, crystal field, and magnetic properties of these systems may serve to clarify unanswered questions in their understanding. In this paper, dc magnetic susceptibility measurements, polarized Raman scattering experiments, and terahertz time domain spectroscopy on aforementioned members of the rare earth titanates family are employed to gain more insights into the details that drive them toward such diverse behaviors. Raman scattering allows for simultaneous investigation of structural and CF properties through the observation of both phononic and CF excitations, while the comparison between the various members helps to identify the nature of the different excitations observed.

II. EXPERIMENT

A. Sample preparation

Polycrystalline samples of $R_2Ti_2O_7$ (where R=Gd,Tb, Dy,Ho) were synthesized by firing stoichiometric amounts of high purity (>99.9%) TiO_2 and the appropriate rare earth oxide (Gd_2O_3, Tb_4O_7, Dy_2O_3, or Ho_2O_3, respectively) in air for several days with intermittent grindings. The resulting polycrystalline powder was subsequently prepared for single-crystal growth, using the method described by Gardner *et al.*[53] The following single-crystal growth (also done as described in Ref. 53) using the floating zone technique yielded large, high quality single crystals of all of the $R_2Ti_2O_7$ variants. Disks ($\simeq 1$ mm thickness) with (a,b)-plane surfaces were cut from oriented single crystals and subsequently polished, in order to optimize scattering experiments. The $Tb_2Ti_2O_7$ sample used in Raman experiments was subsequently polished down to $\simeq 250$ μm thickness to facilitate terahertz transmission measurements.

B. Instrumentation

X-ray Laue diffraction, using a Philips PW 1710 diffractometer equipped with a Polaroid XR-7 system, was employed to orient the single-crystal samples of $Gd_2Ti_2O_7$ and $Tb_2Ti_2O_7$ for the polarized Raman spectroscopy experiments, while simultaneously confirming the single crystallinity of the samples. The $Dy_2Ti_2O_7$ and $Ho_2Ti_2O_7$ single crystals were oriented using an Enraf-Nonius CAD4 diffractometer.

The magnetic susceptibilities of the obtained rare earth titanates were measured using the Quantum Design MPMS-5 superconducting quantum interference device (SQUID) magnetometer of the Laboratoire de Physico-Chimie de l'Etat Solide (LPCES) at the Université Paris-Sud in Orsay, France. The $R_2Ti_2O_7$ samples, about 100 mg of single crystal (in the form of disks of approximately 4 mm diameter and 1 mm thickness), were placed in cylindrical plastic tubes and

locked in position. Next, the samples were zero-field cooled down to 1.7 K, after which the magnetization of the sample was measured as a function of the temperature in an applied magnetic field of 100 Oe while warming the sample.

Polarization controlled, inelastic light-scattering experiments were performed on all oriented $R_2Ti_2O_7$ samples. The experiments were performed in a 180° backscattering configuration, using a triple-grating micro-Raman spectrometer (T64000 Jobin Yvon), consisting of a double-grating monochromator (acting as a spectral filter) and a polychromator which disperses the scattered light onto a liquid-nitrogen-cooled charge coupled device (CCD) detector. The frequency resolution was better than 2 cm^{-1} for the frequency region considered. The samples were placed in a liquid-helium-cooled optical flow cryostat (Oxford Instruments). The temperature was stabilized within an accuracy of 0.1 K in the whole range of measured temperatures (from 2.5 to 295 K). The 532.6 nm (frequency doubled) output of a $Nd:YVO_4$ laser was focused onto the $Gd_2Ti_2O_7$, $Tb_2Ti_2O_7$, and $Dy_2Ti_2O_7$ samples using a 50× microscope objective and used as excitation source in the scattering experiments. A krypton laser (676.4 nm) was used as the excitation source for the scattering experiments on the $Ho_2Ti_2O_7$ sample, since 532.6 nm excitation (resonant at low temperatures in case of $Ho_2Ti_2O_7$) results in fluorescence dominating the inelastic-scattering spectrum in the 5–800 cm^{-1} spectral range. The power density on the samples was on the order of 50 $\mu W/\mu m^2$ in all cases. The polarization was controlled on both the incoming and outgoing beams. Parallel (∥) and perpendicular (⊥) measurements on $Gd_2Ti_2O_7$ and $Tb_2Ti_2O_7$ were performed along crystallographic axes of the (a,b) surface of the samples, Porto notations $c(aa)c$ and $c(ab)c$, respectively. Unfortunately, the orientation of the a and b axes in the (a,b) plane of the $Dy_2Ti_2O_7$ and $Ho_2Ti_2O_7$ surfaces with respect to the light polarizations was not known. Analogous Porto notations are $c(xx)c$ (∥) and $c(xy)c$ (⊥), respectively, where x is a direction in the (a,b) plane of the sample making an undetermined angle α with the a axis, while y, in the same (a,b) plane of the crystal, is perpendicular to the x direction. Raman spectra were fitted with Lorentzian line shapes to extract mode parameters.

Terahertz time domain spectroscopy (TTDS) (Ref. 54) was performed on $Tb_2Ti_2O_7$ using a homemade setup similar to those described elsewhere.[54,55] Terahertz pulses (pulse duration of several picoseconds, frequency range of 0.3–2.5 THz) were generated through a difference frequency generation process in a ZnTe single crystal upon pulsed excitation (120 fs, 800 nm) by an amplified Ti:sapphire system. The magnitude of the time dependent electric field transmitted through the sample (with respect to. that transmitted through vacuum) was measured at various temperatures through electro-optic sampling in a second ZnTe single crystal using 800 nm pulses of approximately 120 fs. The sample used was a thin slice of single crystalline $Tb_2Ti_2O_7$ (the same sample used in the Raman experiments), which was mounted on a copper plate with an aperture (∅2 mm) and placed in a liquid-helium-cooled optical flow cryostat (Oxford Instruments). The polarization of the terahertz radiation was parallel to the crystallographic a axis.

III. RESULTS AND DISCUSSION

A. Magnetic measurements

The magnetic susceptibility χ, defined as the ratio of the magnetization of the sample to the applied magnetic field, of all the rare earth titanate samples was measured in a 100 Oe applied magnetic field. Since the samples used were platelike disks, the data have been corrected by a demagnetization factor as calculated for flat, cylindrical plates.[56] Figure 1 shows the inverse molar susceptibilities of all samples in the low-temperature regime. For each sample, the data were fitted to a Curie-Weiss form for the molar magnetic susceptibility of an antiferromagnet,

$$\chi_m = \frac{2C}{(T-\theta)} + B, \tag{1}$$

where C is the Curie constant in cgs units ($C=N_A\mu^2\mu_B^2/3k_b \simeq \mu^2/8$, in [emu K mol^{-1}]), θ is the expected transition temperature (which gives an indication of the sign of the magnetic interactions), and B is a temperature independent Van Vleck contribution to the susceptibility. The model was fitted to high-temperature experimental data (100 K and up, where the demagnetization correction is on the order of 1%). Linear regression analysis of $\chi_{m,i}^{-1}$ yielded the experimental values for θ_i, μ_i, and B_i. These are tabulated in Table I, together with several values reported in literature.

In general, the experimentally obtained data compare (where possible) favorably to the various values reported in literature (Table I). The extracted θ parameters for $Dy_2Ti_2O_7$ and $Ho_2Ti_2O_7$ do slightly deviate from literature values, presumably due to the estimation of the demagnetization factor, which is larger in these materials (fits to uncorrected data yield θ values of approximately 1 and 2 K). The experimentally determined paramagnetic moments obtained for $Gd_2Ti_2O_7$ and $Tb_2Ti_2O_7$ are also in excellent agreement with the corresponding free ion values, which are $\mu=7.94\mu_B$ and $\mu=9.72\mu_B$ for the Gd^{3+} ($^8S_{7/2}$) and Tb^{3+} ($^7F_6$) free ions, respectively. The large negative Curie-Weiss temperatures for $Gd_2Ti_2O_7$ and $Tb_2Ti_2O_7$ indicate antiferromagnetic exchange coupling. In contrast, the small, positive θ values for $Ho_2Ti_2O_7$ and $Dy_2Ti_2O_7$ initially led to the assumption of weak ferromagnetic exchange interactions between nearest-neighbor Dy^{3+} and Ho^{3+} ions.[42] As stated above, however, since the Ho^{3+} and Dy^{3+} ions have a large magnetic moment [free ion values are $\mu=10.607\mu_B$ ($^5I_8$ ground state) and $\mu=10.646\mu_B$ ($^6H_{15/2}$ ground state)], the dipolar interactions between neighboring R^{3+} ions are dominating the effective nearest-neighbor (nn) interactions. The nn *exchange* interactions are in fact *anti*ferromagnetic,[43] while the dominant dipolar nn interactions are of ferromagnetic nature.[28,44] Consequently, the effective nn interactions are slightly ferromagnetic, resulting in the positive θ values. Another consequence of the dipolar interactions and their dominance is the fact that extracting the real values of μ and B from the inverse susceptibility curves becomes nontrivial, since more elaborate models taking the dipolar interaction into account are needed.

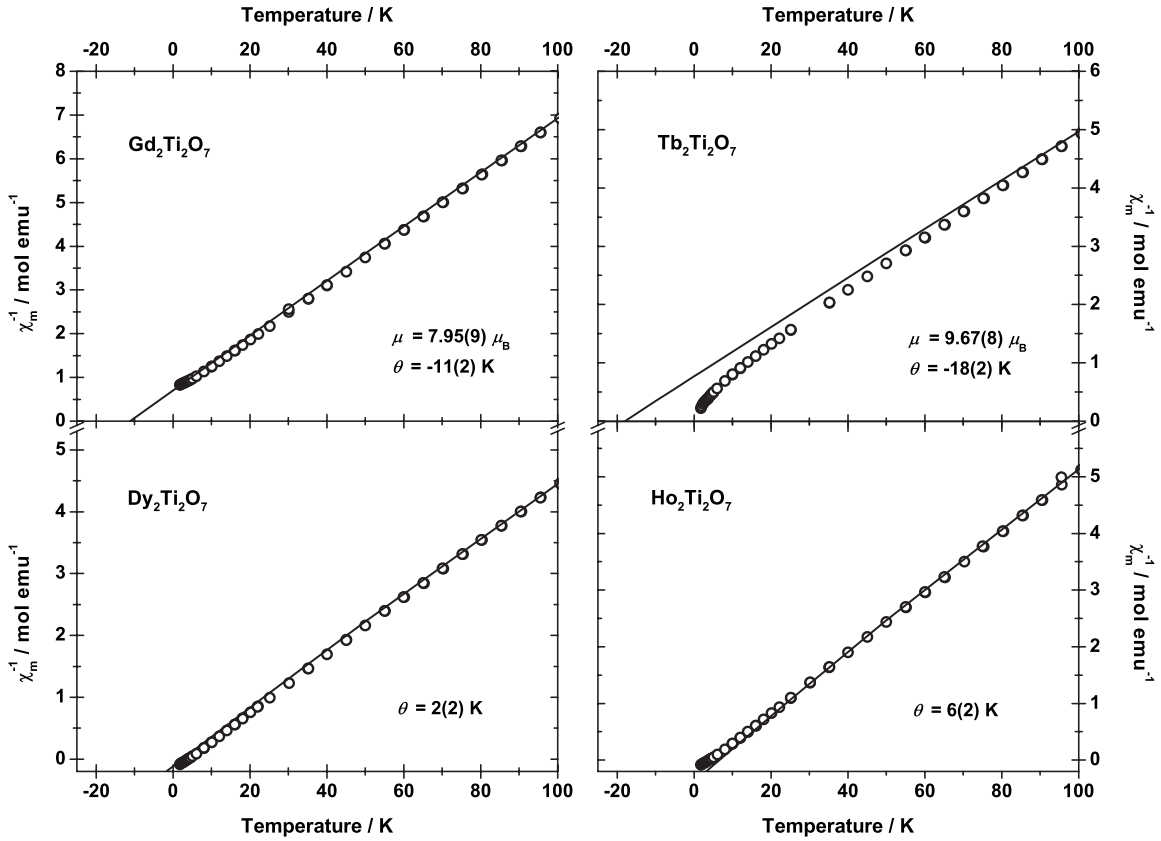

FIG. 1. Inverse molar magnetic susceptibilities (open circles) of all $R_2Ti_2O_7$ samples and their corresponding Curie-Weiss fits [solid lines, Eq. (1)] versus temperature. The Curie-Weiss law, which is fitted to the higher-temperature data (>100 K), is obeyed down to low temperatures.

B. Raman spectroscopy

1. Room-temperature spectra

To determine the Raman-active vibrations of the single crystals, group theory analysis was employed. This predicts that for the cubic rare earth titanate structure ($R_2Ti_2O_7$) of space group $Fd\bar{3}m$ (O_h^7), the sublattices of the unit cell span the following irreducible representations:

$$16(c)\ \text{site: Ti}^{4+}\ \text{sublattice} = A_{2u} + E_u + 2F_{1u} + F_{2u},$$

$$16(d)\ \text{site: } R^{3+}\ \text{sublattice} = A_{2u} + E_u + 2F_{1u} + F_{2u},$$

$$48(f)\ \text{site: O(1)}\ \text{sublattice} = A_{1g} + E_g + 2F_{1g} + 3F_{2g} + A_{2u} + E_u + 3F_{1u} + 2F_{2u},$$

$$8(a)\ \text{site: O(2)}\ \text{sublattice} = F_{1u} + F_{2g}.$$

This makes the following decomposition into zone-center normal modes (excluding the F_{1u} acoustic mode):

$$\Gamma = A_{1g} + E_g + 2F_{1g} + 4F_{2g} + 3A_{2u} + 3E_u + 7F_{1u} + 4F_{2u}.$$

Of these normal modes, only the A_{1g}, E_g, and the four F_{2g} modes are Raman active. The seven F_{1u} modes are infrared active and the remaining modes are optically inactive. The symmetry coordinates for the optically active normal modes are given by Gupta *et al.*[57] Based on the symmetries of the Raman-active modes, the A_{1g} and E_g modes are expected to be observed in parallel polarization ($\parallel$) spectra, while the F_{2g} modes are expected in the perpendicular polarization ($\perp$) spectra. Surprisingly, the room-temperature spectra of $R_2Ti_2O_7$ show all the Raman-active modes in both polariza-

TABLE I. Experimentally determined and literature values for θ_i, μ_i, and B_i for the different $R_2Ti_2O_7$ compounds. The numbers inside parentheses give the accuracy in the last digit of the values.

Compound i (source)	θ_i (K)	μ_i (μ_B)	B_i (emu mol^{-1})
$Gd_2Ti_2O_7$ (expt.)	−11(2)	7.95(9)	0[a]
$Gd_2Ti_2O_7$ (Ref. 13)	−9.6	7.7	
$Gd_2Ti_2O_7$ (Ref. 14)	−11.7	7.8	
$Gd_2Ti_2O_7$ (Ref. 42)	−8.95(6)	7.224(3)	6.0×10^{-4}
$Tb_2Ti_2O_7$ (expt.)	−18(2)	9.67(7)	$3.4(9)\times10^{-3}$
$Tb_2Ti_2O_7$ (Refs. 21 and 22)	−19	9.6	
$Dy_2Ti_2O_7$ (expt.)	2(2)	[b]	[b]
$Dy_2Ti_2O_7$ (Ref. 42)	≃1.0	9.590(6)	$1.1(1)\times10^{-2}$
$Ho_2Ti_2O_7$ (expt.)	6(2)	[b]	[b]
$Ho_2Ti_2O_7$ (Ref. 42)	≃2.0	9.15(3)	$1.2(1)\times10^{-2}$

[a]When fitting χ_m with a nonzero B term, it becomes negligibly small. The best fit is obtained with $B=0$.
[b]Since dipolar interactions are dominant in this case, no reliable values were extracted (see text).

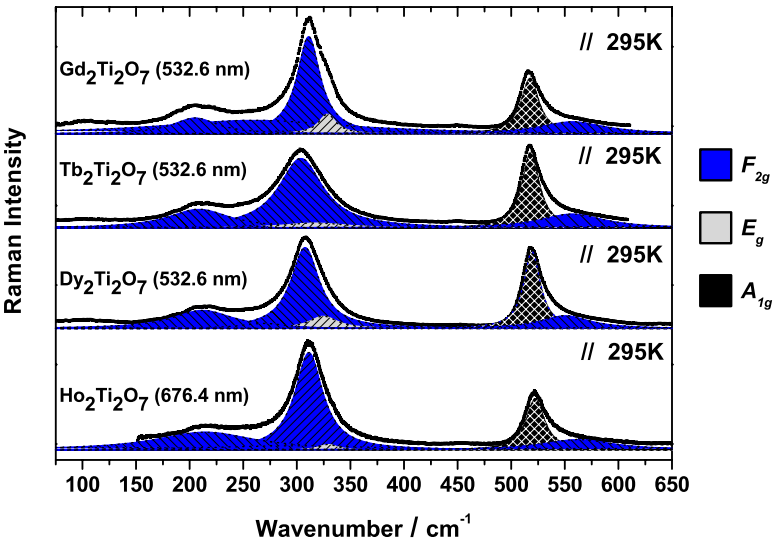

FIG. 2. (Color online) Room-temperature Raman spectra of the $R_2Ti_2O_7$ crystals in parallel polarization configuration. The assignment of the Raman-active modes to the observed peaks is indicated by the filled Lorentzian line shapes.

tions. Angle dependent Raman measurements (varying the angle between the incoming light polarization and the *b* axis from −45° to 45°) reveal no orientation in which the theoretical selection rules are fully obeyed. Polycrystallinity and/or crystalline disorder is, however, not believed to be the cause, since other techniques (x-ray Laue diffraction and magnetic measurements) reveal no such signs. Also, to our best knowledge, no Raman spectrum of any of these rare earth titanates fulfilling their phononic selection rules has been published. Although no full compliance of phononic selection rules was observed, the nature of the Raman-active modes was clearly identified through their angular dependence. Their assignment is indicated in Fig. 2 as well as in Table II. The figure depicts the room-temperature (RT) parallel polarization spectra of the rare earth titanates and the corresponding modes. The assignment of the mode symmetries is based on comparison with assignments in previous works on these[57–62] and related[62–67] compounds (see Table II), on aforementioned measurements (not shown) of the angular dependence of mode intensities and on the temperature dependence of the modes (*vide infra*).

Comparison between the RT Raman spectra yields the conclusion that the nature of the R^{3+} ion has only a slight influence on the Raman-active vibrational modes. This is not surprising since in all the Raman-active modes, only the oxygen atoms are displaced.[57,58] Consequently, there is no obvious systematic variation of the phonon frequencies with the mass of the respective rare earth ions, as has been noted

TABLE II. Experimentally determined and literature values of the frequencies (in cm^{-1}) of observed Raman modes in $R_2Ti_2O_7$ at room temperature and their respective symmetry assignments (inside parentheses).

This work				Ref. 58	Ref. 59	Ref. 60	Ref. 61	Ref. 57		Ref. 62
R=Gd	Tb	Dy	Ho	Gd	Gd	Gd	Gd	Gd (calc.)	Gd (obs.)	Gd
~104[a]	~102[a]	~103[a]	~105[a] (-)	(-)	(-)	105 (F_{2g})	(-)	(-)	(-)	110 (-)
~128[a]		~124[a]	~122[a] (-)	(-)	(-)	125 (-)[b]	(-)	(-)	(-)	215 (-)
205	209	212	214 (F_{2g})	215 (F_{2g})	210 (F_{2g})	222 (F_{2g})	219 (F_{2g})	230.6 (F_{2g})	225 (F_{2g})	225 (F_{2g})
260	256	269	297 (F_{2g})	(-)	(-)	(-)	(-)	(-)	(-)	(-)
310	303	308	311 (F_{2g})	312 (F_{2g})	310[d] (E_g)	311 (E_g)	312 (E_g)	318.0 (E_g)	(-)	317 (F_{2g})
325	313	328	329(E_g)	330 (E_g)	310[d] (F_{2g})	(-)	(-)	328.2 (F_{2g})	317 (F_{2g})	347[e] (E_g)
450[c]	450[c]	451[c]	452[c] (-)	(-)	470 (F_{2g})	452 (-)	455 (F_{2g})	(-)	(-)	(-)
			(-)	(-)	(-)	(-)	(-)	522.2 (F_{2g})	(-)	(-)
517	518	519	522 (A_{1g})	518 (A_{1g}/F_{2g})	520 (A_{1g})	518 (F_{2g})	519 (A_{1g})	526.8 (A_{1g})	515 (A_{1g})	515 ($A_{1g}+F_{2g}$)
554	557	550	562 (F_{2g})	547 (F_{2g})	570 (F_{2g})	585 (F_{2g})	549 (F_{2g})	594.0 (F_{2g})	580 (F_{2g})	580 (F_{2g})
~677[f]	~689[f]	~693[f]	~701[f] (-)	684 (-)	(-)	(-)	680 (F_{2g})	(-)	(-)	(-)
~703[f]	~706[f]	~720[f]	~724[f] (-)	701 (-)	(-)	(-)	(-)	(-)	(-)	705 (-)

[a]These modes are very weak and barely resolved; therefore their exact positions are estimated.
[b]Mori *et al.* (Ref. 60) ascribed this band to trace amounts of Gd_2O_3.
[c]This is a very weak mode, barely resolved above the noise. Mori *et al.* (Ref. 60) ascribed this mode to trace amounts of TiO_2.
[d]Zhang *et al.* (Ref. 59) indicated the lower- and higher-wave-number components of this band as the E_g and F_{2g} modes, respectively.
[e]This band was calculated, rather than observed, by Vandenborre *et al.* (Ref. 62).
[f]These overlapping modes comprise a weak band, in which the two modes cannot be separately resolved.

before for the rare earth titanates,[57] hafnates,[66] manganates,[63] and stannates.[65] The assignment of the $R_2Ti_2O_7$ modes in literature has been mostly consistent (see Table II), yet there are a few debated details. There is general agreement on the nature of the modes at $\simeq$210 cm^{-1} [F_{2g}, O(2)-sublattice mode[58]], $\simeq$519 cm^{-1} (A_{1g},*R*-O stretching mode[59,60]), and $\simeq$556 cm^{-1} [F_{2g}, O(1)-sublattice mode[58]]. Temperature and angle dependent Raman measurements show that the band around $\simeq$315 cm^{-1} consists of two modes, an F_{2g} mode around 310 cm^{-1} (O-*R*-O bending mode[59,60]) and an E_g mode around 327 cm^{-1} [O(1)-sublattice mode[58]], as recognized by Saha *et al.*[58] and Vandenborre *et al.*[67] Earlier works either interchanged the mode assignment within this band[57,59] or ascribed the whole band to only one of these modes.[60,61] However, our temperature and angle dependent measurements confirm the assignment made by Saha *et al.*[58] The last expected phonon, an F_{2g} mode, has been either not accounted for,[57] combined with the A_{1g} mode in one band,[58,62] or ascribed to low intensity peaks around 105,[60] 450,[59] or 680 cm^{-1} (Ref. 61) in previous works. Here, it is ascribed to a broad, low intensity mode around $\simeq$260 cm^{-1}. This mode is not clearly resolved in the RT spectra due to the fact that it overlaps largely with the neighboring strong F_{2g} modes at $\simeq$210 cm^{-1} and $\simeq$309 cm^{-1}. Fitting with those two peaks only, however, does not adequately reproduce the experimental spectral shape in the 200–300 cm^{-1} window. Additionally, as the temperature is lowered, the phonon modes sharpen and the existence of this excitation becomes obvious in the spectra. Also worth noting are the two anomalous modes in $Tb_2Ti_2O_7$ at $\simeq$303 cm^{-1} (F_{2g}) and $\simeq$313 cm^{-1} (E_g), which have lower frequencies and wider line shapes compared to their counterparts in the other isostructural rare earth titanates.

Next to the expected Raman-active vibrations, the spectra in this work show some very weak scattering intensity at low wave numbers (first two rows of Table II), which has been reported before.[60,62] Vandenborre *et al.*[62] were unable to account for this intensity in their calculations, while Mori *et al.*[60] offered the plausible assignment to trace R_2O_3 in the system. The latter assignment is also tentatively adopted here. Mori *et al.* also suggested that the "missing" F_{2g} mode might be responsible for some of this low-wave-number intensity. Additionally, a weak mode is observed at 450 cm^{-1} in most $R_2Ti_2O_7$ compounds, as was also seen before. Zhang *et al.*[59] and Hess *et al.*[61] ascribed the missing F_{2g} mode to this feature. Alternatively, Mori *et al.*[60] interpreted it as being due to trace amounts of starting compound TiO_2, which is known[68] to have a phonon at 447 cm^{-1}. The true origin of this mode is at present unclear. Finally, there is some low intensity scattering at higher wave numbers, around 700 cm^{-1} (last two rows of Table II). This intensity has been observed before[58–62] and is ascribed to forbidden IR modes made active by slight local nonstoichiometry in the system.[58,60]

2. Temperature dependence

Raman spectra of the $R_2Ti_2O_7$ crystals were recorded at temperatures ranging from RT to 4 K. Figure 3 depicts the evolution of both the parallel ($\parallel$) and perpendicular ($\perp$) polarization Raman spectra of the $R_2Ti_2O_7$ crystals with decreasing temperature.

Going down in temperature, several spectral changes occur in the Raman spectra. The evolutions of the phononic excitations with temperature are very similar in the different $R_2Ti_2O_7$ lattices. Again, this is not surprising, since only oxygen atoms are displaced in the Raman-active phonons.[57,58] First, the lowest-frequency phonon (F_{2g}, $\omega \simeq 210$ cm^{-1} at RT) shows a strong softening ($\omega \simeq 170$ cm^{-1} at 4 K) and sharpening with decreasing temperature, revealing the previously unresolved F_{2g} mode ($\omega_{RT} \simeq 260$ cm^{-1}), which also softens ($\omega_{4\ K} \simeq 190$ cm^{-1}), but does not show a strong narrowing. Second, the sharpening of both the $\simeq$309 cm^{-1} F_{2g} and the $\simeq$324 cm^{-1} E_g modes decreases their spectral overlap, clearly justifying the two-mode interpretation of the $\simeq$315 cm^{-1} band at RT. Additionally, both modes show a slight softening upon cooldown. Also, the A_{1g} phonon ($\omega_{RT} \simeq 519$ cm^{-1}) shows the familiar softening ($\omega_{4\ K} \simeq 511$ cm^{-1}) and sharpening trend on cooling. Finally, due to its large width and low intensity, describing the temperature evolution of the highest-frequency F_{2g} phonon proves rather difficult, though it seems to soften slightly. Comparison of the $R_2Ti_2O_7$ spectra in Fig. 3 yields the observation that the anomalous phonons [at $\simeq$303 (F_{2g}) and $\simeq$313 cm^{-1} (E_g)] in $Tb_2Ti_2O_7$ remain wide throughout the temperature range, in contrast to the corresponding modes in the other titanates. Additionally, these modes are shifting in opposite directions in $Tb_2Ti_2O_7$ only: the F_{2g} mode softens ($\omega_{4\ K} \simeq 295$ cm^{-1}), while the E_g mode considerably hardens ($\omega_{4\ K} \simeq 335$ cm^{-1}). An explanation for this anomalous behavior could be the coupling of these phonons to low-frequency crystal field excitations of the Tb^{3+} ions (*vide infra*).

3. Crystal field excitations

Aside from the phonons in the Raman spectra of $R_2Ti_2O_7$, several spectra also show crystal field (CF) excitations of the R^{3+} ions at low temperatures, as shown in Fig. 4. The CF level splitting in the different rare earth ions depends on their electronic configuration and their local surroundings. In the $R_2Ti_2O_7$ family, the simplest case is that of the Gd^{3+} ion ($4f^7$), which has a spin-only $^8s_{7/2}$ ($L=0$) ground state, resulting in the absence of a level splitting due to the local crystal field. Consequently, the Raman spectrum of $Gd_2Ti_2O_7$ shows no CF excitations, making it a suitable "template" of the $R_2Ti_2O_7$ Raman spectrum with lattice excitations only. Combined with the strong correspondence of the phononic excitations in the $R_2Ti_2O_7$ spectra, it allows for quick identification of CF modes in the other compounds.

More complicated is the CF level splitting in the Tb^{3+} ion ($4f^8$), which has a $^7F_6$ ground state. Several studies calculating the crystal field for the Tb^{3+} ion in $Tb_2Ti_2O_7$,[22,25–27] based on inelastic-neutron-scattering results,[21,22,25,27,69,70] yielded slightly differing energy-level schemes for the lowest crystal field levels of Tb^{3+} in $Tb_2Ti_2O_7$ as schematically depicted in Fig. 5. Here, solid lines depict CF levels observed experimentally, while dotted lines indicate CF levels obtained through CF calculations. Shown in Fig. 6, which is a zoom of the low-wave-number region of the 4 K perpendicu-

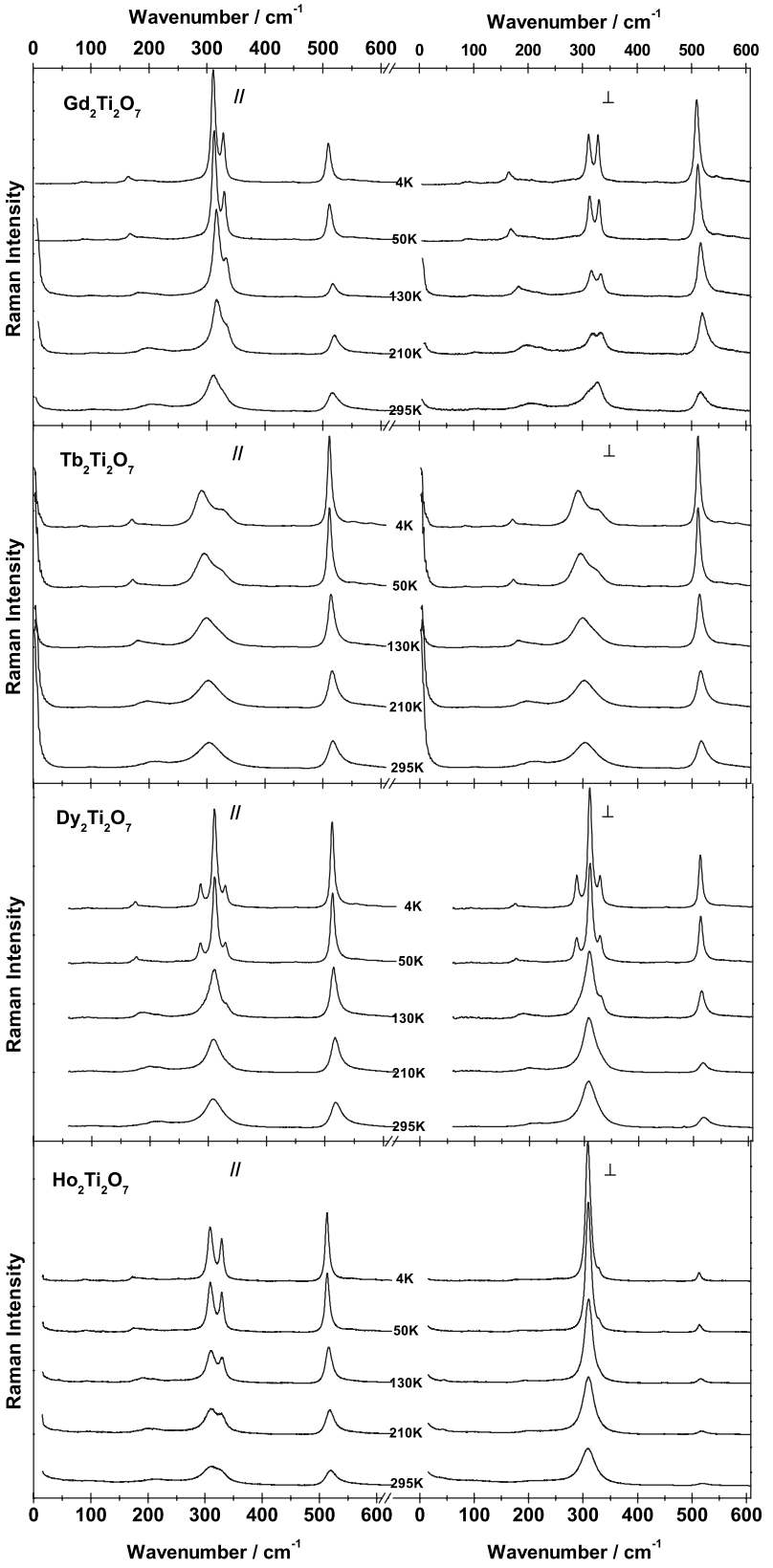

FIG. 3. Temperature dependence of the $R_2Ti_2O_7$ parallel (∥) and perpendicular (⊥) Raman spectra. The spectra show several changes when going down in temperature (see text), most of which (the phononic excitations) are analogous for all $R_2Ti_2O_7$ lattices. In addition, at lower temperatures various crystal field excitations appear in the spectra of some of the rare earth titanates (see Fig. 4). Spectra are normalized to the integrated intensity of the depicted frequency window.

lar polarization spectrum of $Tb_2Ti_2O_7$, are the CF excitations that are observed using inelastic light scattering. As also clear from Fig. 5, all CF excitations previously observed using inelastic neutron scattering are also observed here. Furthermore, additional low-lying excitations can be seen, which are easily identified as CF levels, by comparison with the "lattice-only template" spectrum of $Gd_2Ti_2O_7$.

The excitations from the crystal field ground state to the higher crystal field levels, with approximately calculated values of 13, 60, 83, and 118 cm^{-1} (see Fig. 5), are all observed

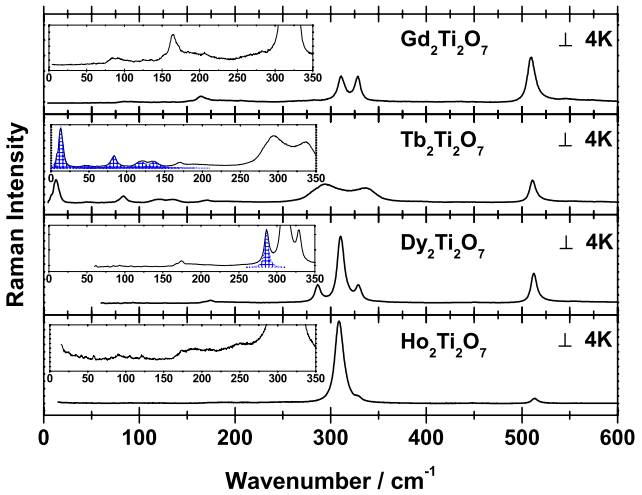

FIG. 4. (Color online) Low-temperature spectra for all $R_2Ti_2O_7$ as measured in perpendicular polarization configuration. The spectra are normalized on the total integrated intensity of the spectra. The insets show respective zooms on the lower-wave-number regions of the spectra, where the excitations identified as CF levels of the rare earth ions are indicated by dotted blue Lorentzian peaks. $Gd_2Ti_2O_7$ shows only phononic modes and can be regarded as the lattice template. $Tb_2Ti_2O_7$ and $Dy_2Ti_2O_7$ show additional CF modes, while $Ho_2Ti_2O_7$ shows again only lattice excitations. A fitted Lorentzian centered at zero (Rayleigh line) is subtracted from the $Tb_2Ti_2O_7$ data for clarity.

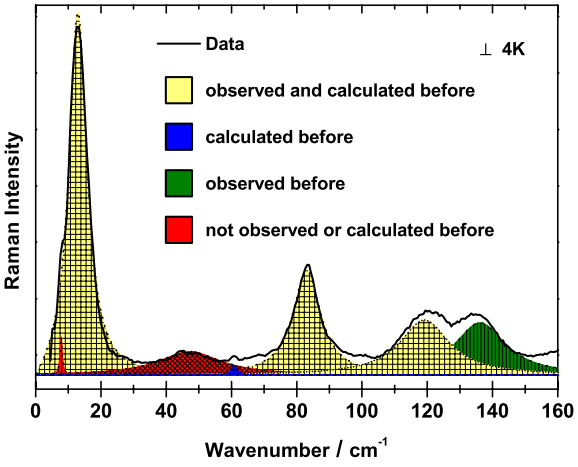

FIG. 6. (Color online) The low-wave-number region of the perpendicular polarization Raman spectrum of $Tb_2Ti_2O_7$ at 4 K. A fitted Lorentzian centered at zero (Rayleigh line) is subtracted from the data for clarity. The crystal field levels (see Fig. 5) are indicated by the filled Lorentzian line shapes that were fitted to the data. A distinction has been made between CF levels that have been calculated and observed before (yellow), CF levels that have been calculated before but so far have not been observed (blue), CF levels that have been observed before but have not been calculated (green), and additional CF levels that are observed in this study using inelastic light scattering (red).

at very similar frequencies, at 12.9, 60.8, 83.1, and 119.2 cm^{-1}, respectively. The 60.8 cm^{-1} level has not been observed experimentally before, though it did follow from the CF calculation made by Gingras *et al.*[22] Conversely, the $\simeq$135.2 cm^{-1} mode has been observed through inelastic neutron scattering yet has not been accounted for in CF calculations. Although Gardner *et al.*[27] interpreted it as an optical phonon, this excitation is clearly identified as a CF excitation here, through the isostructural comparison with the other titanates. The latter assignment was also made by Mirebeau *et al.*[25] Additionally, other CF excitations are observed

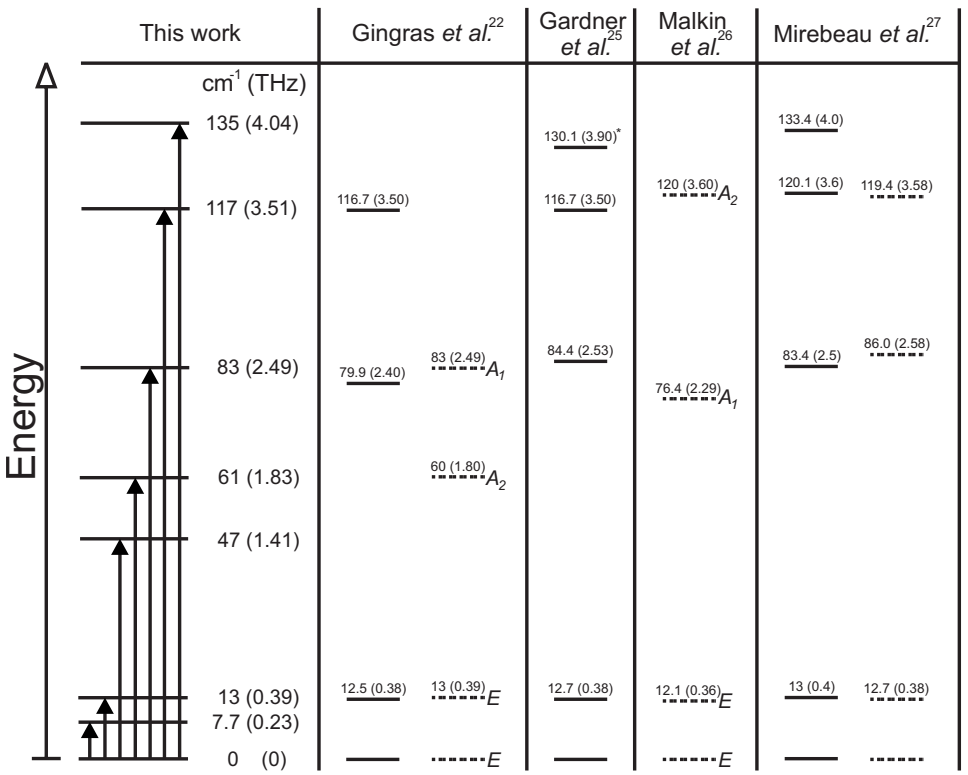

FIG. 5. Various CF energy-level schemes of the Tb^{3+} ion in $Tb_2Ti_2O_7$. Solid lines depict CF levels that have been observed experimentally, while dotted lines represent CF levels as calculated using CF calculations. Numbers indicate CF level energies in cm^{-1} (THz); symbols in italics indicate symmetries of corresponding levels. Solid arrows indicate all CF excitations observed in the low-temperature Raman spectrum of $Tb_2Ti_2O_7$ (see Fig. 6).

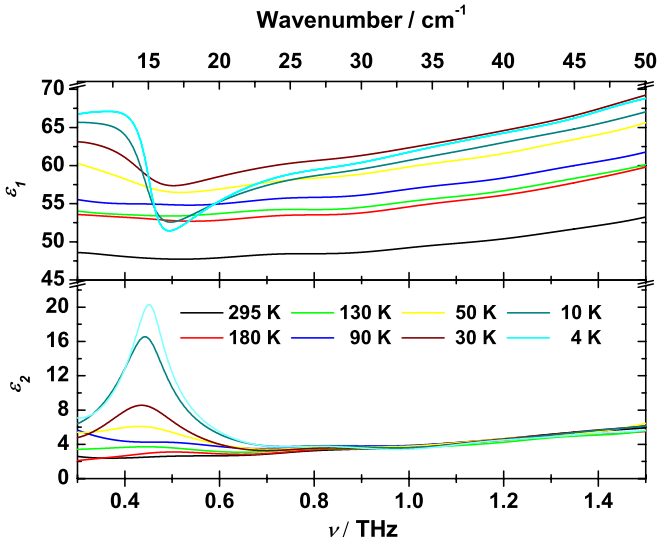

FIG. 7. (Color online) Real (upper panel) and imaginary (lower panel) parts of the complex dielectric constant of $Tb_2Ti_2O_7$ in the terahertz regime. The color legend applies to both panels.

at 7.7 and 47.2 cm^{-1}. While the former is recognized as a CF excitation from the CF ground state to a new CF energy level, the 47.2 cm^{-1} excitation could also be interpreted as an excitation from the excited CF level at 12.9 cm^{-1} to the higher excited CF level at 60.8 cm^{-1}. While such an excitation is Raman active (see below), its occurrence at 4 K seems unlikely, since at this temperature the excited CF level (12.9 $cm^{-1} \simeq 19$ K) is not expected to be populated enough to give rise to a measurable Raman signal. Additionally, if it were an excitation from an excited state, its intensity would decrease upon cooling. Instead, the intensity of this mode steadily increases with decreasing temperature.

Using E_g and E_g, A_{2g} and A_{1g} irreducible representations[22,26] for the ground state and excited CF levels, respectively, it can be confirmed that indeed all these ground state to excited state transitions are expected to be Raman active. Through analogous considerations, the lowest excitation ($E_g \rightarrow E_g$, 13 cm^{-1}) is found to be symmetry forbidden in a direct dipole transition. In this respect, terahertz time domain spectroscopy (TTDS) in the range of 10–50 cm^{-1} (0.3–1.5 THz) was employed to probe the absorption of $Tb_2Ti_2O_7$ at various temperatures. By using this technique, it is possible to extract complex optical quantities in the terahertz range through the direct measurement of the time trace of the transmitted terahertz pulse. The obtained curves for the real $[\epsilon_1(\nu)]$ and imaginary $[\epsilon_2(\nu)]$ parts of the dielectric constant at various temperatures are plotted in Fig. 7. The plots clearly show an absorption around 0.45 THz (15 cm^{-1}) at low temperatures, corresponding to the 13 cm^{-1} CF level also observed in the Raman spectra of $Tb_2Ti_2O_7$. This is corroborated by the identical temperature dependences of the mode in both methods: its spectral signature decreases with increasing temperature, vanishing around 90 K. The fact that the 13 cm^{-1} CF level is observed in a direct dipole transition indicates that this level is not a true $E_g \rightarrow E_g$ transition, since such a dipole transition would be symmetry forbidden.

Overall, the existence of the additional CF levels in $Tb_2Ti_2O_7$, unaccounted for by CF calculations, suggests the presence of a second Tb^{3+} site in the structure with an energy-level scheme different from those reported previously. Three additional CF levels are observed experimentally, while four would naively be expected for a slightly differing Tb site in this low-wave-number region. A fourth additional CF level might be unresolved due to the strong CF level at 83 cm^{-1} or might simply be symmetry forbidden in a Raman transition. Moreover, the fact that the $\sim$13 cm^{-1} CF level is simultaneously Raman and dipole active indicates the breaking of inversion symmetry in the system, which questions the validity of its current symmetry interpretation. Recently, the exact symmetry of the $Tb_2Ti_2O_7$ lattice has been extensively studied. Han *et al.*[71] performed neutron powder diffraction and x-ray absorption fine-structure experiments down to 4.5 K, revealing a perfect pyrochlore lattice, within experimental error. Ofer *et al.*[72] found no static lattice distortions on the timescale of 0.1 μs, down to 70 mK. Most recently, however, Ruff *et al.*[73] found finite structural correlations at temperatures below 20 K, indicative of fluctuations above a very low–temperature structural transition. The present experimental results suggest these fluctuations may even induce a minute static disorder, resulting in the observed CF level diagram.

In $Dy_2Ti_2O_7$ the Dy^{3+} ions ($4f^9$) have a $^6H_{15/2}$ ground state. Crystal field calculations have been performed by Jana *et al.*,[74] who deduced an energy-level scheme consisting of eight Kramers doublets, with a separation of $\simeq$100 cm^{-1} of the first excited state. Malkin *et al.*[26] and Rosenkranz *et al.*[75] estimated the first excited state gap to be $>$200 and $\simeq$266 cm^{-1}, respectively. The Raman spectrum of $Dy_2Ti_2O_7$ shows only one extra excitation compared to the "lattice template" spectrum of $Gd_2Ti_2O_7$, at the energy of $\sim$287 cm^{-1}. This excitation is tentatively ascribed to the first excited CF level, comparing most favorably to the estimation of Rosenkranz *et al.*

For $Ho_2Ti_2O_7$ ground state $^5I_8$ (Ho^{3+},$4f^{10}$), several CF energy-level schemes have been calculated,[26,75–77] all with first excited state separations around 150 cm^{-1}. However, the Raman spectrum of $Ho_2Ti_2O_7$ does not show any clear inelastic light scattering from CF levels to which these calculations can be compared. Although there is some weak intensity around $\simeq$150 cm^{-1}, which compares favorably with all of the calculated level schemes, the intensity of this scattering is insufficient to definitively ascribe it to a CF level.

IV. CONCLUSIONS

To summarize, several members of the rare earth titanates family $R_2Ti_2O_7$ were studied using magnetic susceptibility measurements and polarized inelastic-light-scattering experiments. Lattice excitations were found to vary only slightly between crystals with different rare earth ions. Temperature dependent measurements also revealed completely analogous behaviors of the phononic excitations except for two anomalous phonons in $Tb_2Ti_2O_7$, which seem to be coupled to the low-energy crystal field excitations in that compound. Such crystal field excitations were observed in $Tb_2Ti_2O_7$ and possibly also in $Dy_2Ti_2O_7$. Only one nonphononic excitation is

clearly observed in $Dy_2Ti_2O_7$, its energy consistent with estimates of the first excited crystal field level. For $Tb_2Ti_2O_7$, all of the previously determined crystal field energy levels were confirmed. Moreover, the resulting energy-level diagram was expanded by three additional observed CF levels, only one of which has been calculated before. Also, one previously reported level was found to be both Raman and dipole active, contradicting its current presumed symmetry. These findings may reflect the existence of two inequivalent Tb sites in the low-temperature structure or a static symmetry reduction of another nature, suggesting the recently found structural correlations to induce a minute static disorder in $Tb_2Ti_2O_7$ at very low temperatures. This crystal field information may serve to help elucidate the complex theoretical enigma of $Tb_2Ti_2O_7$.

Note added in proof. Recently, some additional indications of low-temperature structural changes in the rare earth titanates have been found both experimentally[78] and theoretically.[79]

ACKNOWLEDGMENTS

The authors would like to thank F. van der Horst for his help in using the PW 1710 diffractometer. We also acknowledge fruitful discussions with M. Mostovoi, D. Khomskii, and S. Singh. This work is part of the research program of the Stichting voor Fundamenteel Onderzoek der Materie (FOM), which is financially supported by the Nederlandse Organisatie voor Wetenschappelijk Onderzoek (NWO).

*p.h.m.van.loosdrecht@rug.nl

[1] A. P. Ramirez, Annu. Rev. Mater. Sci. **24**, 453 (1994).
[2] P. Schiffer and A. P. Ramirez, Comments Condens. Matter Phys. **18**, 21 (1996).
[3] *Magnetic Systems with Competing Interactions*, edited by H. T. Diep (World Scientific, Singapore, 1994).
[4] J. E. Greedan, J. Alloys Compd. **408-412**, 444 (2006).
[5] J. E. Greedan, J. Mater. Chem. **11**, 37 (2001).
[6] M. F. Collins and O. A. Petrenko, Can. J. Phys. **75**, 605 (1997).
[7] R. Moessner, Can. J. Phys. **79**, 1283 (2001).
[8] J. Villain, Z. Phys. B **33**, 31 (1979).
[9] J. N. Reimers, A. J. Berlinsky, and A. C. Shi, Phys. Rev. B **43**, 865 (1991).
[10] R. Moessner and J. T. Chalker, Phys. Rev. Lett. **80**, 2929 (1998).
[11] J. N. Reimers, Phys. Rev. B **45**, 7287 (1992).
[12] B. Canals and C. Lacroix, Phys. Rev. Lett. **80**, 2933 (1998).
[13] N. P. Raju, M. Dion, M. J. P. Gingras, T. E. Mason, and J. E. Greedan, Phys. Rev. B **59**, 14489 (1999).
[14] J. D. Cashion, A. H. Cooke, M. J. M. Leask, T. L. Thorp, and M. R. Wells, J. Mater. Sci. **3**, 402 (1968).
[15] A. P. Ramirez, B. S. Shastry, A. Hayashi, J. J. Krajewski, D. A. Huse, and R. J. Cava, Phys. Rev. Lett. **89**, 067202 (2002).
[16] J. D. M. Champion, A. S. Wills, T. Fennell, S. T. Bramwell, J. S. Gardner, and M. A. Green, Phys. Rev. B **64**, 140407(R) (2001).
[17] J. R. Stewart, G. Ehlers, A. S. Wills, S. T. Bramwell, and J. S. Gardner, J. Phys.: Condens. Matter **16**, L321 (2004).
[18] A. Yaouanc, P. Dalmas de Réotier, V. Glazkov, C. Marin, P. Bonville, J. A. Hodges, P. C. M. Gubbens, S. Sakarya, and C. Baines, Phys. Rev. Lett. **95**, 047203 (2005).
[19] S. R. Dunsiger, R. F. Kiefl, J. A. Chakhalian, J. E. Greedan, W. A. MacFarlane, R. I. Miller, G. D. Morris, A. N. Price, N. P. Raju, and J. E. Sonier, Phys. Rev. B **73**, 172418 (2006).
[20] S. E. Palmer and J. T. Chalker, Phys. Rev. B **62**, 488 (2000).
[21] J. S. Gardner *et al.*, Phys. Rev. Lett. **82**, 1012 (1999).
[22] M. J. P. Gingras, B. C. den Hertog, M. Faucher, J. S. Gardner, S. R. Dunsiger, L. J. Chang, B. D. Gaulin, N. P. Raju, and J. E. Greedan, Phys. Rev. B **62**, 6496 (2000).
[23] J. S. Gardner *et al.*, Phys. Rev. B **68**, 180401(R) (2003).
[24] S. Rosenkranz, A. P. Ramirez, A. Hayashi, R. J. Cava, R. Siddharthan, and B. S. Shastry, J. Appl. Phys. **87**, 5914 (2000).
[25] I. Mirebeau, P. Bonville, and M. Hennion, Phys. Rev. B **76**, 184436 (2007).
[26] B. Z. Malkin, A. R. Zakirov, M. N. Popova, S. A. Klimin, E. P. Chukalina, E. Antic-Fidancev, P. Goldner, P. Aschehoug, and G. Dhalenne, Phys. Rev. B **70**, 075112 (2004).
[27] J. S. Gardner, B. D. Gaulin, A. J. Berlinsky, P. Waldron, S. R. Dunsiger, N. P. Raju, and J. E. Greedan, Phys. Rev. B **64**, 224416 (2001).
[28] B. C. den Hertog and M. J. P. Gingras, Phys. Rev. Lett. **84**, 3430 (2000).
[29] Y. J. Kao, M. Enjalran, A. Del Maestro, H. R. Molavian, and M. J. P. Gingras, Phys. Rev. B **68**, 172407 (2003).
[30] The ground-state configuration of the spin ice model is formed by satisfying conditions analogous to Pauling's "ice rules:" every tetrahedron has both two spins pointing into and two spins pointing out of the tetrahedron. This (under)constraint on the system again results in a macroscopically large number of degenerate ground states.
[31] H. R. Molavian, M. J. P. Gingras, and B. Canals, Phys. Rev. Lett. **98**, 157204 (2007).
[32] M. Enjalran, M. J. P. Gingras, Y. J. Kao, A. del Maestro, and H. R. Molavian, J. Phys.: Condens. Matter **16**, S673 (2004).
[33] I. Mirebeau, A. Apetrei, I. N. Goncharenko, and R. Moessner, Physica B (Amsterdam) **385-386**, 307 (2004).
[34] S. H. Curnoe, Phys. Rev. B **75**, 212404 (2007).
[35] A. P. Ramirez, A. Hayashi, R. J. Cava, R. Siddharthan, and B. S. Shastry, Nature (London) **399**, 333 (1999).
[36] J. Snyder, B. G. Ueland, J. S. Slusky, H. Karunadasa, R. J. Cava, and P. Schiffer, Phys. Rev. B **69**, 064414 (2004).
[37] A. P. Ramirez, C. L. Broholm, R. J. Cava, and G. R. Kowach, Physica B (Amsterdam) **280**, 290 (2000).
[38] M. J. Harris, S. T. Bramwell, D. F. McMorrow, T. Zeiske, and K. W. Godfrey, Phys. Rev. Lett. **79**, 2554 (1997).
[39] S. T. Bramwell *et al.*, Phys. Rev. Lett. **87**, 047205 (2001).
[40] A. L. Cornelius and J. S. Gardner, Phys. Rev. B **64**, 060406(R) (2001).
[41] O. A. Petrenko, M. R. Lees, and G. Balakrishnan, Phys. Rev. B **68**, 012406 (2003).
[42] S. T. Bramwell, M. N. Field, M. J. Harris, and I. P. Parkin, J. Phys.: Condens. Matter **12**, 483 (2000).

[43] R. G. Melko and M. J. P. Gingras, J. Phys.: Condens. Matter **16**, R1277 (2004).
[44] S. T. Bramwell and M. J. P. Gingras, Science **294**, 1495 (2001).
[45] S. T. Bramwell and M. J. Harris, J. Phys.: Condens. Matter **10**, L215 (1998).
[46] P. W. Anderson, Phys. Rev. **102**, 1008 (1956).
[47] L. Pauling, J. Am. Chem. Soc. **57**, 2680 (1935).
[48] S. V. Isakov, R. Moessner, and S. L. Sondhi, Phys. Rev. Lett. **95**, 217201 (2005).
[49] H. Fukazawa, R. G. Melko, R. Higashinaka, Y. Maeno, and M. J. P. Gingras, Phys. Rev. B **65**, 054410 (2002).
[50] T. Fennell, O. A. Petrenko, G. Balakrishnan, S. T. Bramwell, J. D. M. Champion, B. Fak, M. J. Harris, and D. M. Paul, Appl. Phys. A: Mater. Sci. Process. **74**, S889 (2002).
[51] M. J. Harris, S. T. Bramwell, T. Zeiske, D. F. McMorrow, and P. J. C. King, J. Magn. Magn. Mater. **177-181**, 757 (1998).
[52] G. Ehlers, A. L. Cornelius, T. Fennell, M. Koza, S. T. Bramwell, and J. S. Gardner, J. Phys.: Condens. Matter **16**, S635 (2006).
[53] J. S. Gardner, B. D. Gaulin, and D. M. Paul, J. Cryst. Growth **191**, 740 (1998), and references therein.
[54] C. A. Schmuttenmaer, Chem. Rev. (Washington, D.C.) **104**, 1759 (2004).
[55] M. C. Beard, G. M. Turner, and C. A. Schmuttenmaer, Phys. Rev. B **62**, 15764 (2000).
[56] M. Sato and Y. Ishii, J. Appl. Phys. **66**, 983 (1989).
[57] H. C. Gupta, S. Brown, N. Rani, and V. B. Gohel, J. Raman Spectrosc. **32**, 41 (2001).
[58] S. Saha, D. V. S. Muthu, C. Pascanut, N. Dragoe, R. Suryanarayanan, G. Dhalenne, A. Revcolevschi, S. Karmakar, S. M. Sharma, and A. K. Sood, Phys. Rev. B **74**, 064109 (2006).
[59] F. X. Zhang and S. K. Saxena, Chem. Phys. Lett. **413**, 248 (2005).
[60] M. Mori, G. M. Tompsett, N. M. Sammes, E. Suda, and Y. Takeda, Solid State Ionics **158**, 79 (2003), and references therein.
[61] N. J. Hess, B. D. Begg, S. D. Conradson, D. E. McCready, P. L. Gassman, and W. J. Weber, J. Phys. Chem. B **106**, 4663 (2002).
[62] M. T. Vandenborre and E. Husson, J. Solid State Chem. **50**, 362 (1983).
[63] S. Brown, H. C. Gupta, J. A. Alonso, and M. J. Martinez-Lope, J. Raman Spectrosc. **34**, 240 (2003).
[64] M. Glerup, O. F. Nielsen, and W. F. Poulsen, J. Solid State Chem. **160**, 25 (2001).
[65] H. C. Gupta, S. Brown, N. Rani, and V. B. Gohel, Int. J. Inorg. Mater. **3**, 983 (2001).
[66] H. C. Gupta, S. Brown, N. Rani, and V. B. Gohel, J. Phys. Chem. Solids **63**, 535 (2002).
[67] M. T. Vandenborre, E. Husson, J. P. Chatry, and D. Michel, J. Raman Spectrosc. **14**, 63 (1983).
[68] S. P. S. Porto, P. A. Fleury, and T. C. Damen, Phys. Rev. **154**, 522 (1967).
[69] B. D. Gaulin, J. S. Gardner, S. R. Dunsiger, Z. Tun, M. D. Lumsden, R. F. Kiefl, N. P. Raju, J. N. Reimers, and J. E. Greedan, Physica B (Amsterdam) **241-243**, 511 (1997).
[70] M. Kanada, Y. Yasui, M. Ito, H. Harashina, M. Sato, H. Okumura, and K. Kakurai, J. Phys. Soc. Jpn. **68**, 3802 (1999).
[71] S. W. Han, J. S. Gardner, and C. H. Booth, Phys. Rev. B **69**, 024416 (2004).
[72] O. Ofer, A. Keren, and C. Baines, J. Phys.: Condens. Matter **19**, 145270 (2007).
[73] J. P. C. Ruff, B. D. Gaulin, J. P. Castellan, K. C. Rule, J. P. Clancy, J. Rodriguez, and H. A. Dabkowska, Phys. Rev. Lett. **99**, 237202 (2007).
[74] Y. M. Jana, A. Sengupta, and D. Ghosh, J. Magn. Magn. Mater. **248**, 7 (2002).
[75] S. Rosenkranz, A. P. Ramirez, A. Hayashi, R. J. Cava, R. Siddharthan, and B. S. Shastry, J. Appl. Phys. **87**, 5914 (2000).
[76] R. Siddharthan, B. S. Shastry, A. P. Ramirez, A. Hayashi, R. J. Cava, and S. Rosenkranz, Phys. Rev. Lett. **83**, 1854 (1999).
[77] Y. M. Jana and D. Ghosh, Phys. Rev. B **61**, 9657 (2000).
[78] M. Maczka, J. Hanuza, K. Hermanowicz, A. F. Fuentes, K. Matsuhira, and Z. Hiroi, J. Raman Spectrosc. **39**, 537 (2008).
[79] S. H. Curnoe, arXiv:0712.1703v1 (unpublished).